

**COMPARISON OF NEUTRON IRRADIATION EFFECTS ON CAST AND  
PM-HIP GRADE 91 STEELS**

by

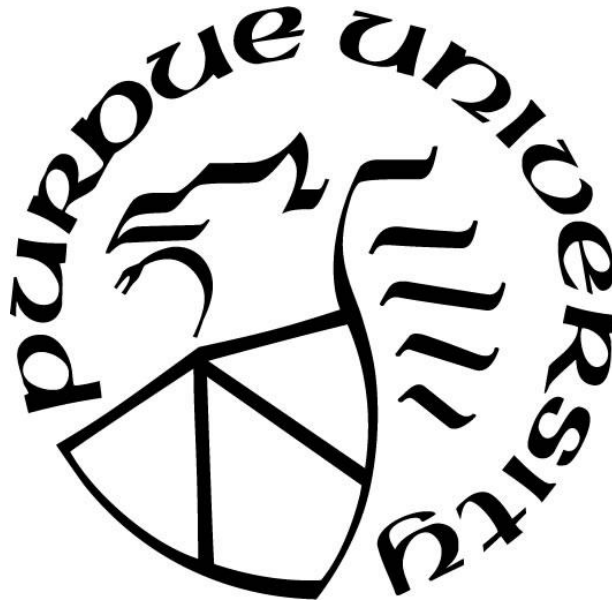
**Sri Sowmya Panuganti**

**A Thesis**

*Submitted to the Faculty of Purdue University*

*In Partial Fulfillment of the Requirements for the degree of*

**Master of Science in Materials Engineering**



School of Materials Engineering

West Lafayette, Indiana

May 2022

**THE PURDUE UNIVERSITY GRADUATE SCHOOL  
STATEMENT OF COMMITTEE APPROVAL**

**Dr. Janelle Wharry, Chair**

School of Materials Engineering

**Dr. Maria Okunewski**

School of Materials Engineering

**Dr. Nikilesh Chawla**

School of Materials Engineering

**Approved by:**

Dr. David F. Bahr

To my parents,  
Sudha and Balakrishna Panuganti  
And  
To my brother and sister,  
Chaitanya and Shiva  
And all my family and friends,  
Thank you for supporting me through everything

## ACKNOWLEDGMENTS

I would like to thank my advisor Dr. Janelle Wharry, for all of her support, patience, motivation and guidance throughout this process. I would also like to thank my committee members.

I would also like to thank the staff at CAES Dr. Yu Lu - thank you for helping with all of the STEM and APT work. I would also like to thank Dr. Yaqiao Wu for data collection, and general guidance on the APT software. I would like to thank Dr. Rosa Diaz for all of her time training me on TEM and Sotoudeh Sedaghat for her time training me on the FIB.

I would like to thank my group members Amrita Sen, Caleb Clement, Yangyang Zhao, who have helped me with research, studies and given me lots of grad school advice. I would also like to thank my friends Ochithyaa, Akhil, Ari, Devika, Dominique, Iris, Ava, Maggie, Lotanna, Geetha, Vaidehi, Sisco, Brian, DipDip and the rest of my friends for having my back and supporting me through these last two years.

I also want to thank my parents, brother, Subha, Hymys, Mihir, Icu, Nidhi and the rest of my family for their continued support and love. Finally, I want to thank my grandfather, U.V.G Rao, who has always fostered and inspired my interest in science.

# TABLE OF CONTENTS

LIST OF TABLES .....	6
LIST OF FIGURES .....	7
LIST OF ABBREVIATIONS.....	8
ABSTRACT.....	9
1. INTRODUCTION .....	10
2. BACKGROUND .....	11
2.1 Ferritic/Martensitic Steels (F/M steels) .....	11
2.2 PM-HIP Processing.....	13
2.3 Strengthening Models .....	14
3. METHODS .....	20
3.1 Sample Preparation .....	20
3.2 Tensile Testing.....	20
3.3 Atom Probe Tomography (APT) .....	20
3.4 STEM.....	21
4. RESULTS .....	26
4.1 Tensile Test Results .....	26
4.2 STEM Characterization Results.....	26
4.3 Atom Probe Tomography Results.....	28
5. DISCUSSION.....	38
5.1 Increase in Yield Stress.....	38
5.2 Strengthening Calculations .....	38
5.3 Si Segregation .....	40
6. CONCLUSION & FUTURE WORK.....	42
APPENDIX: SUPPLEMENTARY FIGURES.....	43
REFERENCES .....	47

## LIST OF TABLES

Table 3.1. Composition of G91 steel in this study.....	22
Table 4.1. Tensile test results.....	29
Table 4.2. Summary of Dislocation loop measurements. ....	29
Table 4.3. Summary of dislocation line data .....	30
Table 4.4. Summary of APT reconstruction data. ....	31
Table 5.1. Summary of strengthening calculations.....	41

## LIST OF FIGURES

Figure 2.1. Schematic of microstructure of typical F/M alloy.....	17
Figure 2.2. TEM micrographs of F82H (a) and T91(b) [14]. .....	18
Figure 2.3. Orowan model shows dislocations bowing around defects.....	19
Figure 3.1. Schematic of tensile bar sample. ....	23
Figure 3.2. Schematic of ATR where samples were subject to irradiation.....	24
Figure 3.3. SEM image of where Pt layer was placed on PM-HIP sample. ....	25
Figure 4.1. Stress- strain curves, where the cast is the green lines and PM-HIP is purple.....	32
Figure 4.2. BFSTEM images of unirradiated Cast sample. ....	33
Figure 4.3. BFSTEM images of PM-HIP unirradiated sample.....	33
Figure 4.4. BFSTEM images of irradiated Cast sample. ....	34
Figure 4.5. BFSTEM images of irradiated PM-HIP sample.....	34
Figure 4.6. APT reconstructions of Cast R33_10784 tip.....	35
Figure 4.7. APT reconstructions of PM-HIP R33_21502, shows slight Ni precipitation and Si segregation. ....	36
Figure 4.8. APT reconstructions of PM-HIP tip that shows significant Si segregation. ....	37

## LIST OF ABBREVIATIONS

APT	Atom Probe Tomography
ATR	Advanced Test Reactor
BCC	Body Centered Cubic
BCT	Body Centered Tetragonal
BFSTEM	Bright Field Scanning Transmission Electron Microscopy
BKS	Bacon- Kocks- Scattergood Model
CAES	Center for Advanced Energy Studies
DBH	Dispersed Barrier Hardening
DBTT	Ductile to Brittle Transition Temperature
F/M	Ferritic-Martensitic
FIB	Focused Ion Beam
FKH	Friedel-Kroupa-Hirsch Model
G91	Grade 91 Steel
INL	Idaho National Lab
ODS	Oxide Dispersion Strengthened
PAGB	Prior Austenitic Grain Boundaries
PM-HIP	Powder Metallurgy Hot Isostatic Pressing
RIS	Radiation Induced Segregation
SH	Source Hardening
STEM	Scanning Transmission Electron Microscopy

## **ABSTRACT**

In recent years Powder Metallurgy Hot Isostatic Pressing (PM-HIP) alloys have been of interest to the nuclear power industry to replace alloys fabricated through typical manufacturing processes. However, irradiation effects on PM-HIP alloys have not yet been thoroughly researched. These alloys offer many advantages over typically cast alloys such as more uniform microstructures, higher quality, ease of inspectability, and lower costs. Gaining a better understanding of the evolution of the microstructure under various irradiation conditions is important. The objective of this thesis is to compare irradiation effects on Grade 91 steel that has been cast and produced by PM-HIP. Samples were subjected to fast spectrum neutron irradiation at the Advanced Test Reactor (ATR) at Idaho National Lab (INL). They were irradiated at 400°C to 1 dpa.

Tensile testing was conducted on both irradiated and unirradiated samples to quantify the increase in yield stress due to irradiation. General microstructure characterization was conducted through Scanning Transmission Electron Microscopy (STEM) on both irradiated and unirradiated samples, this allows for a better understanding of dislocation evolution and the effect dislocation loops have on strengthening. Atom Probe Tomography (APT) was utilized to create three-dimensional reconstructions of the samples to characterize the precipitates that have formed and to gain a better understanding of how those precipitates aid in strengthening. Various strengthening models are then applied to understand how each of these defects affects the increase in yield strength in this alloy. The PM-HIP alloy exhibits higher strengthening due to irradiation compared to the cast alloy, therefore increasing the interest in this type of manufacturing for nuclear applications.

# 1. INTRODUCTION

Ferritic-Martensitic (F/M) alloys have been used as structural materials in many different reactor types, they are a common alternative to austenitic stainless steels. Since ferritic steels corrode significantly slower than austenitic stainless steels, they are more compatible with coolant materials in reactors[1]. F/M alloys also have better creep strengths than typical commercial alloys. They handle thermal stresses better, so have longer lifetimes in use[2].

Most parts for light water reactors are created through traditional process like casting, forging, extrusion and drawing. Powder metallurgy hot isostatic pressing (PM-HIP) has been suggested as an alternative to those traditional processing methods in the nuclear power industry. This process could be used to create high quality, uniform parts that can improve the operation and safety of nuclear reactors. PM-HIP alloys have been suggested for use in light water reactors, small modular reactors, and in Gen IV reactors as well. But currently there is not much characterization on the irradiation response of PM-HIP alloys. The purpose of this work is to better understand how these alloys change under irradiation and compare these changes to those in alloys made from a traditional processing method.

Gaining a better understanding on how PM-HIP microstructures change under irradiation could make them more viable for widespread use in reactors. The process does have benefits as far as mechanical properties and cost, as opposed to traditional methods. Understanding how this processing affects post-irradiation microstructure, also allows for tailoring these alloys more closely to industry needs. The purpose of this work is characterizing the microstructure of PM-HIP alloys after irradiation as compared to a traditional processing method.

## 2. BACKGROUND

### 2.1 Ferritic/Martensitic Steels (F/M steels)

Ferritic/Martensitic steels have been used in nuclear applications for tube end fittings and evaporator parts since the early 1970s. They were also used for steam generators in the 1960s [3]. These alloys are made with higher chromium contents (9-12%) and are alloyed with other elements such as Mo, Nb, V, Si, and W[4]. High chromium steels are also alloyed with lower amounts of C, between 0.1-0.2%. These steels tend to have good corrosion resistance and superior strength[3]. They also have acceptable creep strengths at moderate temperature ranges. High chromium steels are often used to repair leaks in the welds between various parts of steam tubes and plates [3]. High Cr steels are also advantageous over austenitic stainless steels because they have lower swelling rates and retain decent mechanical properties [5]. These properties make this class of steels of high interest for nuclear applications.

As mentioned previously these alloys typically contain various different elements that can help optimize their function. For example, Mo is added as it can help increase creep strength through solid solution strengthening. Si may cause void growth, as it is an undersized atom. Too large of an addition of Si can however decrease the oxidation resistance. Alloying with V, N, and Ti can often lead to precipitates like VC, VN, TiC to form. Elements like Al, Si and V can help also raise the ductile to brittle transition temperature, which would be beneficial to increase the range in which the alloy could be in use[6], [7]. In general, changes in DBTT are a large concern with neutron irradiation because embrittlement would decrease the fracture toughness. With high chromium steels, however, in the operating temperature range dose does not markedly change the DBTT[3], [8].

Some commonly used F/M steels are 9Cr-1Mo, HT9, T91. They are often found as cladding steels, or wrapper steels in fast breeder reactors [1]. Grade 91 steel is one such ferritic/martensitic high chromium steel. It was developed in the late 1970's by Oak Ridge National Lab. It generally has around 9 wt% Cr and 1 wt% Mo. The original purpose for this steel was going to be used in steam generators, where the temperatures would not be above 550°C[9].

### 2.1.1 F/M Steels Microstructure

F/M steels are iron based and can have a BCC or BCT crystal structure. Most high Cr steels (12Cr and 9Cr) tend to have  $M_{23}C_6$  carbides that form. If there is a very low C content and 9% Cr there tends to be none of these carbides[10], [11]. These precipitates are shown in Figure 2.1 from literature[11]. These steels have a martensitic lath structure, and prior austenite grain boundaries (PAGB) [12]. Lath boundaries and PAGB contain MX precipitates and  $M_{23}C_6$  these act pins for grain boundaries and prevent sliding, therefore aiding in creep resistance[13], [14]. Figure 2.2. TEM micrographs of F82H (a) and T91(b) [14].

shows some common microstructures of F/M steels, F82H and T91[14]. F/M steels also tend to have high dislocation densities which are results of the martensitic transformation[2].

### 2.1.2 Irradiation Effects of F/M Steels

Irradiation damage occurs when particles like neutrons, protons, ions or electrons dislocate atoms from their original positions. This is a common problem for materials that are used in fuel cladding, reactor walls, and bolts[1],[7]. The process is often called a displacement cascade, as the atoms that are displaced will cause their neighbors to also be displaced. Each displacement event will cause a vacancy and interstitial, which result in “irradiation effects” in the material [3]. Since reactors operate at higher temperatures these (vacancies and interstitials) are able to move and will often recombine. If there are vacancies and interstitials that do not combine, and do not annihilate at sinks they cause damage which affects the mechanical properties of the material. These interstitials can form dislocation loops, cavities, voids, and even precipitates.

The type of damage that can occur depends mainly on the irradiation temperature, generally above one third of the homologous melting temperature is a critical point for damage to occur and accumulate. At temperatures greater than  $0.3T_m$  vacancies and interstitials are generally mobile. In F/M steels there are typically two types of dislocation loops that can form, with burgers vectors of  $a\langle 100 \rangle$  and  $a/2\langle 111 \rangle$ . As mentioned before, cavities can form from vacancies and can cause the material to swell and expand. Cavities can occur in the form of bubbles and voids[1],[7].

Ni/Si/Mn rich precipitates are commonly found irradiation induced precipitates in F/M steels, these are generally dubbed “G phase” precipitates[16],[11]. In F/M alloys these G phase precipitates tend to grow in size with increasing irradiation as shown in a summary provided by

Swenson [16]. Most high chromium steels also tend to have  $\alpha'$  precipitates, which are chromium rich precipitates [16][18]. If there is a high enough Cu content within the alloy, that will also precipitate[19], [20].

Another commonly seen phenomenon is Radiation Induced Segregation (RIS). This is when the solutes in the alloy redistribute themselves as a result of irradiation at higher temperatures. As mentioned before the point defects and clusters that are produced from irradiation become mobile at higher temperatures. Clusters tend to nucleate on pre-existing defects in the material. These defects would then prefer to move to locations like surfaces, grain boundaries, and dislocations, as these acts as defect sinks[21]–[23]. There is a lot less data and understanding on RIS in F/M alloys, so it is harder to predict. Currently studies on these alloys have observed Cr segregation and depletion at grain boundaries depending on conditions [24], [25]. Enrichment and depletion at certain a feature is dependent on the interaction of the elements with the defect flux.

## **2.2 PM-HIP Processing**

The powder metallurgy hot isostatic pressing method of processing was first developed in the 1950's. The process is essentially applying isostatic pressure at elevated temperatures. This allows the powders to become consolidated[26]. There are four main steps to the PM-HIP process. First a three-dimensional model of the component must be created. Then powders must be created through gas atomization. During the gas atomization process a stream of liquid metal is disturbed by the addition of gas[27]. The gas to metal ratio mainly what determines the particle sizes. Powders are sieved and blended to ensure size uniformity[27][28]. Then the powders are packed into the can, that was created in the first step. Care must be taken when filling the powers into the mold as distortion can occur if not [3]. This container is then heated, and isostatic pressure is applied simultaneously, which allows for densification of the powders. After the pieces is consolidated it can be removed and sand blasted for a better finish[3].

There are many benefits to the PM-HIP process over the tradition casting/forging route. PM-HIP allows for the creation of more complex parts, with more uniform microstructures. Parts created through this process are also much easier to remove from the work piece without causing distortion as compared to forged parts. Powder metallurgy also allows more tailoring of exact chemistries [27]. Additionally, as PM-HIP processes produce uniform microstructures they need less repairs than cast counterparts. The hot isostatic pressing process can also be utilized on cast

components to after creation to eliminate porosity. In general PM-HIP components need less post-processing to eliminate defects than traditional casting routes[26], [27].

Currently there are not too many studies that have been conducted on F/M alloys manufactured through PM-HIP that have been subjected to neutron irradiation. Van Osch et al conducted a study on an F82H rolled plate that was processed through PM-HIP and irradiated at 300°C to 2.5-5 dpa [29]. While they saw no difference in the ductile to brittle transition temperature of the PM-HIP sample, it was observed to have a lower upper shelf energy.

Other teams have studied neutron irradiation response of a PM-HIP and traditionally processed SA508 alloy[30]. Their study focused on comparing the irradiation response of bainite and ferrite within the alloy. While this is not an F/M alloy, it does contain quite a bit of ferrite, and therefore is useful to examine in the context of G91. The authors found clustering of Mn-Si-Ni in both bainite and ferrite samples, there was a higher proportion of these clusters in the ferrite sample. Through nanoindentation they found that both the ferrite and bainite regions displayed similar hardness values post irradiation.

Another study conducted by Jong et al analyzed the post-irradiation microstructure of a martensitic stainless steel that was produced through hot isostatic pressing (HIP)[31]. The HIP process was carried out at 1030 °C. The authors analyzed a PH13-8Mo sample that was irradiated from doses of 1.66 to 2.55 dpa at 200 and 300°C. Tensile results of the two irradiation temperatures showed similar ultimate tensile strengths, but varying yield strengths. They attribute this larger change in yield strength for the 200 °C from more radiation damage at lower temperatures [31]. This is due to less thermal processes being active at the lower temperature. The authors also found that fatigue crack propagation was not affected by the irradiation. They, however, did not compare these results to a traditional casting process. Their purpose was mainly to characterize irradiation temperature effects on this HIP alloy.

### **2.3 Strengthening Models**

As plastic deformation occurs in a material, the flow strength of materials can be increased by impeding the movement of dislocations. This is done by the dislocations interacting with various obstacles[32]. This interaction is shown in **Error! Reference source not found.**[33]. In irradiated materials these obstacles tend to be voids, dislocation loops, precipitate and radiation induced segregation[21]. As dislocations interact with these obstacles, they may either bow out or

shear and loop around the obstacles. Both types of interactions increase the yield stress of the material as it requires more energy for the dislocations to move with these obstacles. Various models, discussed below, have been suggested for different dislocation- obstacle interactions.

### 2.3.1 DBH model

The dispersed barrier hardening (also known as Orowan hardening model) is often used to quantify the increase in yield strength due to various obstacles present in the material. The general model is shown below, in Equation 2.1.

$$\Delta\sigma_y = \alpha M\mu b\sqrt{Nd} \quad (2.1)$$

Where  $\alpha$ ,  $M$ ,  $\mu$ ,  $b$  are the strength factor, Taylor factor (3.06), shear modulus, and burgers vector respectively.  $N$  is the number density of obstacles and  $d$  is the size of the obstacles. The strength factor  $\alpha$  varies with the type of barrier that is present. It can range from 0-1 for perfectly weak to perfectly hard barriers[21], [34]. The strength factor is not able to be measured experimentally and there is no clear classification for which barriers have which strength factors[35]. Tan and Busby have created models based on obstacle geometry. They included models for different strengthening mechanisms as well [35].

### 2.3.2 Source Hardening Model

Another model that has been suggested is source hardening (SH). It is seen in both irradiated and unirradiated metals[21]. In the case of irradiation hardening, SH accounts for the dislocation loops (or other features) that decorate dislocation lines[36]. This mechanism will cause a yield drop to be present in the stress-strain curve. This is due to a higher stress that is required for the dislocation to unlock itself from those loops[21][36]. This model accounts for the unlocking that needs to happen of the loops from the dislocation lines. The unlocking stress formula is shown below in Equation 2.2.

$$\sigma_{un} = 0.1 M\mu \left(\frac{b}{l}\right) \left(\frac{d}{y}\right)^2 \quad (2.2)$$

Here  $y$  is the distance from the dislocation line, and  $l$  is the length of that dislocation segment.

### 2.3.3 Other Strengthening Models

While DBH and SH are the two main models to account for irradiation hardening, other variations of those models have also been proposed. Bacon, Kocks and Scattergood proposed a model (BKS model) with a fixed strength factor[37], [38]. The model is shown below in Equation 2.3.

$$\tau_{crss} = h_d \left( \frac{\mu b}{2\pi l} \right) \left[ \ln \left( \frac{l}{b} \right) \right]^{-1/2} \left[ \ln \left( \frac{d'}{b} \right) + 0.7 \right]^{3/2} \quad (2.3)$$

Here  $d' = dl/(d + l)$ , this is a more accurate model for strong models[37].

For weak obstacles Friedel-Kroupa-Hirsch (FKS) model can be used, when dislocations shear these obstacles[39], [40]. The model is shown below in Equation 2.4:

$$\tau_{crss} = \frac{1}{8} h_d (\mu b) N^{2/3} d \quad (2.4)$$

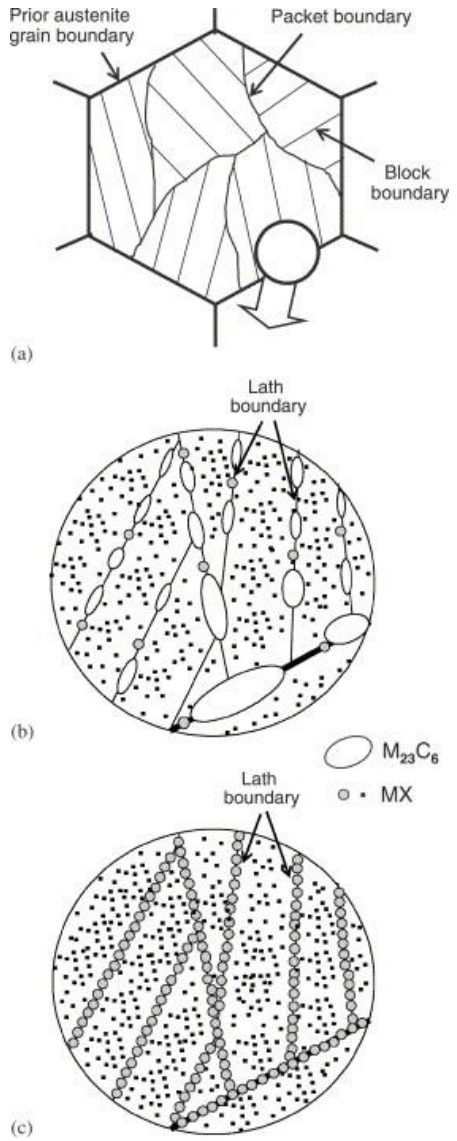


Figure 2.1. Schematic of microstructure of typical F/M alloy.

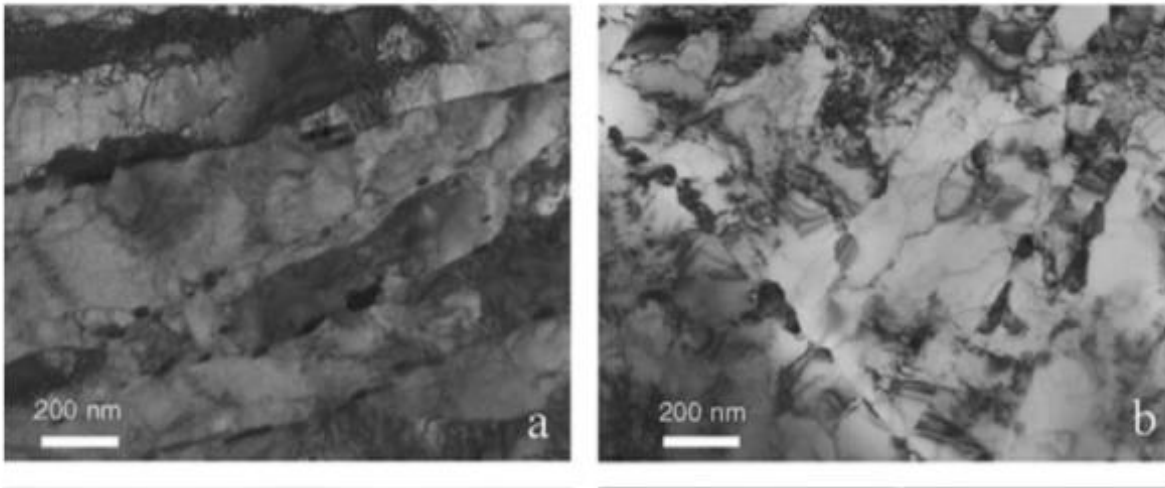


Figure 2.2. TEM micrographs of F82H (a) and T91(b) [14].

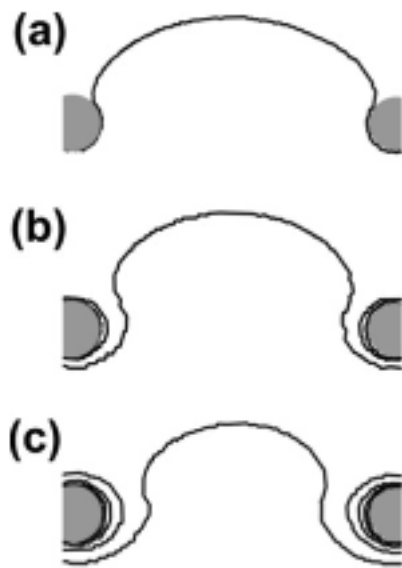


Figure 2.3. Orowan model shows dislocations bowing around defects.

## 3. METHODS

### 3.1 Sample Preparation

Two samples were created, one through PM-HIP processing and the other through a traditional casting process, they were provided by the Electric Power Research Institute (EPRI). The composition of the alloy is shown in [Error! Reference source not found.](#)

The unirradiated specimens were polished to a mirror finish using an auto polisher with SiC paper through 1600 grit. The samples were then vibratory polished for around three hours. Samples were then ultrasonicated to remove any residual polishing liquid. The neutron irradiated TEM discs were electropolished at CAES. The samples were electropolished in a Struers Tenupol-5 A 12.5% perchloric acid solution was used at a temperature of  $-17.5^{\circ}\text{C}$  with a voltage of 18V.

### 3.2 Tensile Testing

Tensile samples were created with a gauge length of 31.75mm and a diameter of 0.25mm, the schematic of these samples is shown in Figure 3.1. Schematic of tensile bar sample. . They were placed in drop in capsules and irradiated in the Advanced Test Reactor (ATR) at Idaho National Laboratory (INL), in the position shown in Figure 3.2. Schematic of ATR where samples were subject to irradiation.. The samples were irradiated to 1 dpa at  $400^{\circ}\text{C}$ . ASTM E8 standard method was followed for tensile testing [41]. Testing was performed at room temperature in an argon environment with the 13M Instron load frame inside the hot cell at the Materials and Fuels Complex (MFC). The crosshead speed was set to 0.27900 mm/min for the samples. Both the irradiated and the as received samples were tested under the same conditions.

### 3.3 Atom Probe Tomography (APT)

Atom probe tomography was also conducted on the irradiated PM-HIP and forged Grade 91 to reconstruct and characterize the clusters. The samples were created by taking a lift out from a random area of the microstructure and sectioning it into several tips. The needles were fabricated using the FEI Quanta 3D FIB at CAES[42]. A 0.4 micron layer of Pt was deposited on the sample

and a sample wedge was lifted out. A final finish beam energy of 2kV and current of 27pA were used. Those wedges were then sectioned into several tips.

The needles for both samples were then run in the Cameca Local Electrode Atom Probe (LEAP) 400x HR at CAES. A pulse frequency of 200 kHz was used at a temperature of 45K with a laser energy of 60 pJ. Data sets were then reconstructed using the Integrated Visualization and Analysis Software (IVAS) Version 3.8.6. Reconstructions in IVAS were created using the procedure outlined by Swenson and Wharry [43]. Image reconstructions were also done through the use of AP Suite 6 from Cameca.

### 3.4 STEM

Microstructure characterization was focused on dislocation loops and lines, and clusters. Dislocation loops and lines were analyzed through scanning transmission electron microscopy (STEM). STEM lamellas were created for all four specimen conditions through the use of focus ion beam milling. The STEM lift outs of the samples of the neutron-irradiated 1dpa 400<sup>0</sup>C were from across grain boundaries, as shown in [Error! Reference source not found.](#). The TEM lamella were prepared using the FEI Quanta 3D FIB at CAES[42]. A 3 micron Pt layer was deposited on the surface as a protective layer. Ga<sup>+</sup> ions were used for bulk milling and the lamella was around 12 microns in length with a depth of 10 micron. Ga<sup>+</sup> ions were also used for thinning to get the thickness less than 100nm. FEI TECNAI G2 FEG STEM (now ThermoFisher) was used for imaging in the Bright-Field Stem (BFSTEM) imaging mode with a camera length of 4.5 m.

For the as received samples STEM lift outs were chosen from random areas of the microstructure. The Helios G4 UX dual beam SEM/FIB at Purdue University was used for lift outs[42]. A 13 x 3 x 4 um Pt protective layer was deposited, and bulk milling was done using Si ions at 30 kV and currents ranging from .11 to 2.4 nA. The lamellas were then welded to a Cu grid and thinned to ~100 nm using Si ions. For BFSTEM characterizations of the unirradiated samples, imaging was done using the ThemisZ TEM at Purdue University, with a camera length of 2.85 m.

Table 3.1. Composition of G91 steel in this study.

C(%)	Si(%)	Mn(%)	P(%)	S(%)	Cr(%)	Ni(%)	Mo(%)	V(%)	N(%)	Nb(%)	Al(%)	Ti(%)	Fe(%)
0.08-0.12	0.2-0.5	0.3-0.6	Max 0.02	Max 0.01	8.0-9.5	Max 0.4	0.85-1.05	0.18-0.25	0.03-0.07	0.06-0.10	Max 0.02	Max 0.01	Bal

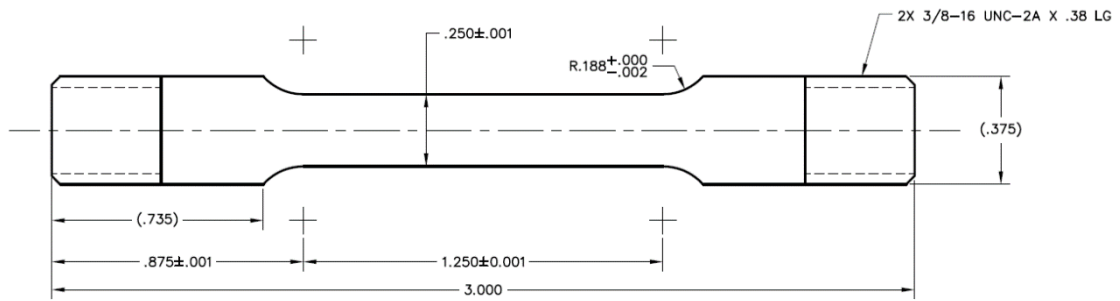


Figure 3.1. Schematic of tensile bar sample.

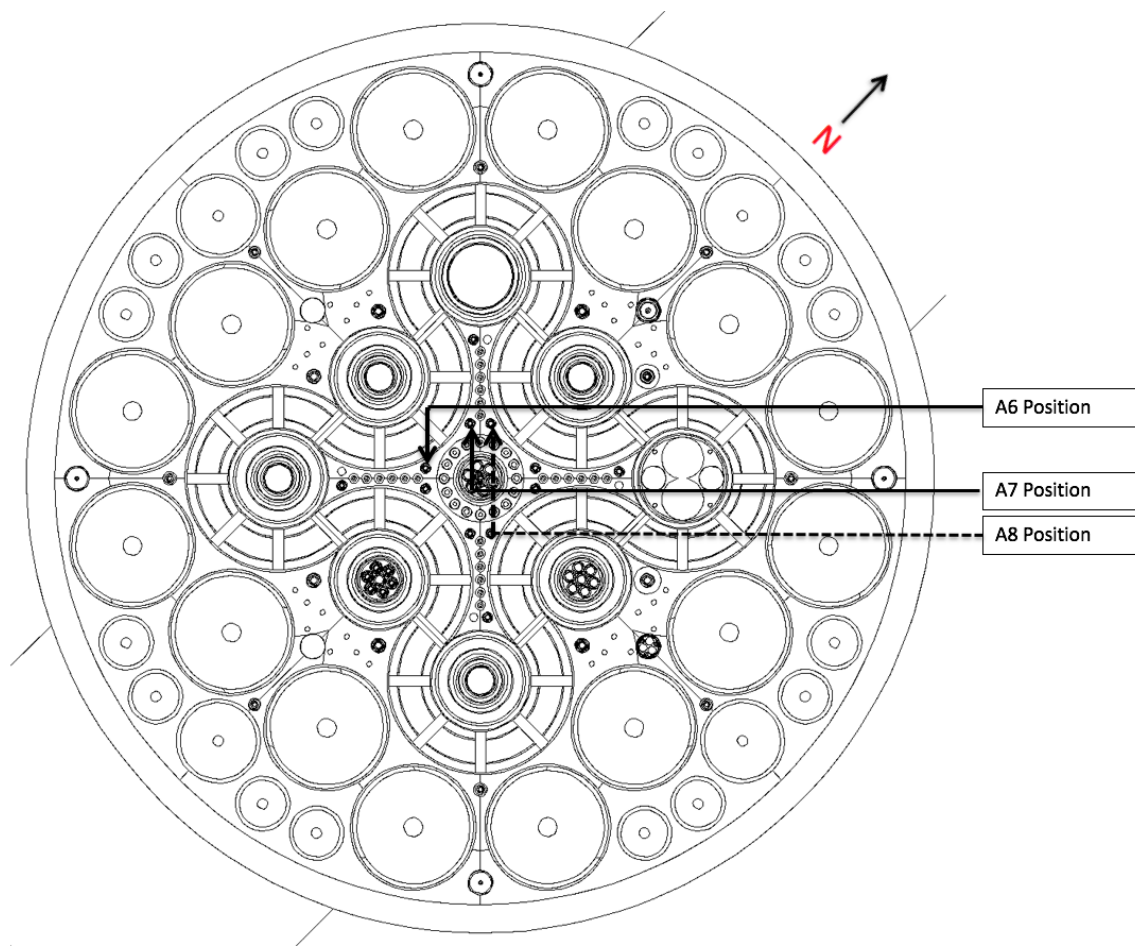


Figure 3.2. Schematic of ATR where samples were subject to irradiation.

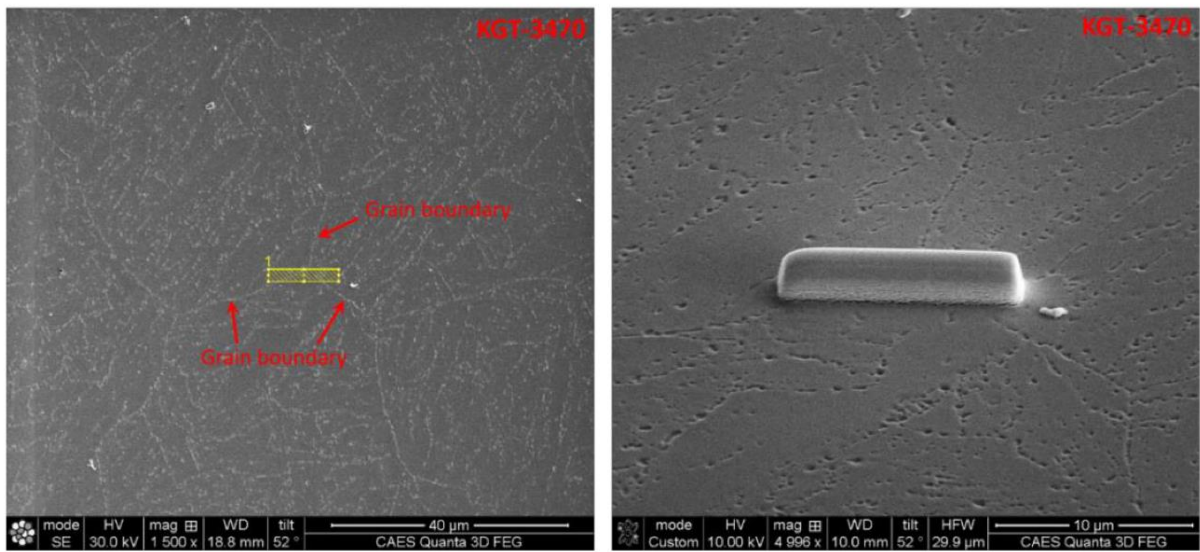


Figure 3.3. SEM image of where Pt layer was placed on PM-HIP sample.

## 4. RESULTS

### 4.1 Tensile Test Results

The tensile test results for both the irradiated and unirradiated samples are shown in **Error! Reference source not found.** The as received cast and PM-HIP had yield strengths of 384.4 MPa and 452.1 MPa respectively. These values were within an expected range for the alloy. Their ultimate tensile strengths (UTS) were quite similar. The as received PM-HIP sample displayed significantly more elongation than the as received cast sample. It can be seen that the yield strengths for the Cast and PM-HIP samples are pretty close in value. The results of the tensile testing are summarized below in **Error! Reference source not found.**

It can also be seen that irradiation results in an increase in YS and UTS in the material, as expected. This difference can be quantified and attributed to various strengthening mechanisms that will be explored in Chapter 5. Here the irradiated PM-HIP material has a longer elongation than the cast alloy as well. In both the irradiated and unirradiated case the PM-HIP sample seems to be more ductile than the Cast material. It is also important to note the yield drop present in both tensile data for the PM-HIP and cast. This feature is often seen with Cottrell atmospheres, however in irradiated materials it is most likely attributed to the unlocking of defects from dislocation line segments as discussed previously in Chapter 2 [36]. As expected, the irradiated materials displayed more embrittlement than the as received counterparts.

### 4.2 STEM Characterization Results

As mentioned previously in Chapter 3. BFSTEM images were taken of the unirradiated samples and are shown in **Error! Reference source not found.** and **Error! Reference source not found.**, which are the Cast and PM-HIP samples respectively. It can be seen in the Cast and PM-HIP samples that there is a similar number density of dislocation lines all of a similar length in both. A few dislocation loops were observed as well but not many. The PM-HIP sample also displayed what could be a pore and areas with smaller dislocation lines. The unirradiated PM-HIP sample showed many areas of heterogeneity as shown in **Error! Reference source not found.** One can see shorter dislocation lines, that almost resemble a eutectic structure. These shorter dislocation lines persist in the microstructure even after irradiation. As expected,

the as-received samples did not display any precipitates or many dislocation loops that would be caused by irradiation. The few dislocation loops that were present may be attributed to processing.

The irradiated Cast BFSTEM images are shown in **Error! Reference source not found.** It can be seen clearly that there are very long dislocation lines that are decorated by dislocation loops. The Cast sample displays more of these loops homogeneously spread through the microstructure. The irradiated PM-HIP BFSTEM images are shown in **Error! Reference source not found.** The PM-HIP sample shows some loops that are distributed throughout the microstructure, but not as distinct decoration of dislocation lines.

#### 4.2.1 Dislocation Loops

As seen in both of the irradiated samples, Cast and PM-HIP, there are a significant amount of dislocation loops present in the microstructure. These dislocation loops can act as obstacles for plastic deformation and aid in increasing the yield strength. Therefore, it is important to be able to quantify the dislocation loops, to then be able to apply them in a strengthening model. The BFSTEM images of dislocation loops were analyzed using ImageJ software to measure their diameters. It was seen that the loops had an average diameter of 24.69 nm and 10.14 nm in the cast and PM-HIP alloys respectively. The cast sample also had almost three times the number density of loops,  $7.62 \times 10^{21}/\text{m}^3$ , than the PM-HIP sample, which was  $2.33 \times 10^{21}/\text{m}^3$ . These results are summarized in Table 4.2. Summary of Dislocation loop measurements.

Table 4. 3. Summary of dislocation line data. Table 4. 4.

Bergner et al, conducted neutron irradiation on several alloys with varying Cr contents. In the 9% Cr alloy that was irradiated to 0.6 dpa they found loops with a mean size of 4 nm, which is significantly smaller than the loops found in this work[36]. Similar alloys at other irradiation conditions, like Sencer et. al found in a HT9 alloy that was neutron irradiated at 443°C reaching doses around 155 dpa, had loops with an average size of 18 nm, which is somewhat more comparable to the loops found in this G91 F/M alloy[28].

#### 4.2.2 Dislocation Lines

Various lengths of dislocation lines were also observed in both the cast and PM-HIP irradiated microstructures. Both samples displayed shorter dislocation lines (less than 200nm in length) and longer lines. The average short line lengths in both samples were very similar as were the average long line lengths. The number density of both types of dislocation lines, short

and long, was higher in the PM-HIP alloys. This is also reflected in the increase in yield strength in the irradiated samples being greater in PM-HIP than in the Cast. As mentioned before, the PM-HIP alloy displayed less distinct decoration of dislocation loops around any lines, as was seen in the cast material. However, both displayed a yield drop, in the tensile results, that could be indicative of dislocations unlocking, as mentioned before. These results are summarized in **Error! Reference source not found..**

### 4.3 Atom Probe Tomography Results

#### 4.3.1 Cast Reconstructions

The APT reconstructions showed distinct precipitates in both types of alloys. For the cast alloy two of the tips that were run contained a sufficient number of ions to be analyzed. One of the tips referred to as R33\_10784 in **Error! Reference source not found.** contained Si, Mn, Ni, VC, and VN in its clusters. The reconstruction of this tip is shown in **Error! Reference source not found.** The other cast tip is referred to as R33\_10793 in Table 4.4 contained the same but, did not have VC. The cast tips had an average radius of 2.255 nm and a number density of  $4.851 \times 10^{22} / \text{m}^3$ . The clusters seem to be fairly homogeneously distributed throughout the reconstruction. The composition of the clusters seems to be heavier in Si, Mn, Ni than the other elements. This indicates those precipitates are most likely the G-phase precipitates.

#### 4.3.2 PM-HIP Reconstructions

Of the first round of PM-HIP samples that were run the tips R33\_10777 and R33\_10746 contained Ni, Mn, Si and P, and Ni and Si respectively. As seen in the Table 4.4 those two tips also had the highest average precipitate radius size. Of the second round of tips that were run the precipitates mainly contained Ni and some also had small amounts of Mn and Si. On average the radius of the precipitates was higher in the first round of tips. The average PM-HIP tip radius was 1.801 nm, which is smaller than that of the cast. The difference in precipitate chemistry could be due to the lift outs of the tips being taken from two random areas of the sample. Of the clusters seen they were not homogeneously distributed throughout the tips. This would indicate that the microstructure was quite heterogeneous after irradiation. The summary of results for PM-HIP and Cast APT reconstructions is in Table 4.4.

It was also seen that in almost all of the PM-HIP tips, shown in **Error! Reference source not found.**, there is significant Si segregation. Rather than being present in the precipitates it seems that the silicon has decorated either dislocations in the microstructure or grain boundaries. It can also be seen that the Si has segregated to almost a plane like structure in the tip, in **Error! Reference source not found.** More on the impact of this Si segregation will be discussed in the following chapter.

Table 4.1. Tensile test results.

Specimen ID	Material	Fabrication Method	Load at Yield (N)	Max. Load (N)	Yield Strength (MPa)	UTS (MPa)	UE (%)	TE (%)
<b>Irradiated</b>	Grade 91	PM-HIP	20686.7	23328.4	653.2	736.6	8.6	19.4
<b>Irradiated</b>	Grade 91	PM-HIP	20873.4	23337.2	659.1	736.9	9.0	21.3
<b>Irradiated</b>	Grade 91	Cast	19126.9	23237.2	604.0	733.8	5.7	13.0
<b>Irradiated</b>	Grade 91	Cast	21221.8	23476.6	670.1	741.3	6.9	16.8
<b>Unirradiated</b>	Grade 91	PM-HIP	15228.0	20247.3	384.4	639.3	10.0	25.7
<b>Unirradiated</b>	Grade 91	Cast	14318.7	19147.1	452.1	604.6	7.1	12.6

Table 4.2. Summary of Dislocation loop measurements.

	Cast	PM-HIP
Avg loop diam (nm)	24.6935	10.1482
Loop # density (#/m <sup>3</sup> )	7.62043 x 10 <sup>21</sup>	2.3311 x 10 <sup>21</sup>

Table 4.3. Summary of dislocation line data

	<b>Cast</b>	<b>PM-HIP</b>
Short line avg (nm)	59.7168	57.2992
Short line # density (#/m <sup>2</sup> )	5.90977 x 10 <sup>13</sup>	8.78729x 10 <sup>13</sup>
Long line avg (nm)	303.9622	255.0008
Long line # density (#/m <sup>2</sup> )	3.39004x 10 <sup>12</sup>	7.17825x 10 <sup>12</sup>

Table 4.4. Summary of APT reconstruction data.

R33_10793	Si, Mn,Ni, VN	$4.157 \times 10^{22}$	0.001562	2.03
Average		$4.851 \times 10^{22}$	0.002821	2.255
<b>PM HIP</b>	<b>Elements in cluster</b>	<b>Density Precipitates (/m<sup>3</sup>)</b>	<b>Volume Fraction</b>	<b>Avg Radius (nm)</b>
R33_21502	Ni	$3.055 \times 10^{22}$	0.0005664	1.457
R33_21475	Ni	$7.582 \times 10^{22}$	0.0004238	1.592
R33_10777	Ni, Mn, Si, P	$4.662 \times 10^{23}$	0.0022447	1.817
R33_21474	Ni,Mn	$7.171 \times 10^{22}$	0.0005719	1.760
R33_10746	Ni, Si	$2.001 \times 10^{23}$	0.004293	2.377
Average		$1.687 \times 10^{23}$	0.001619	1.801

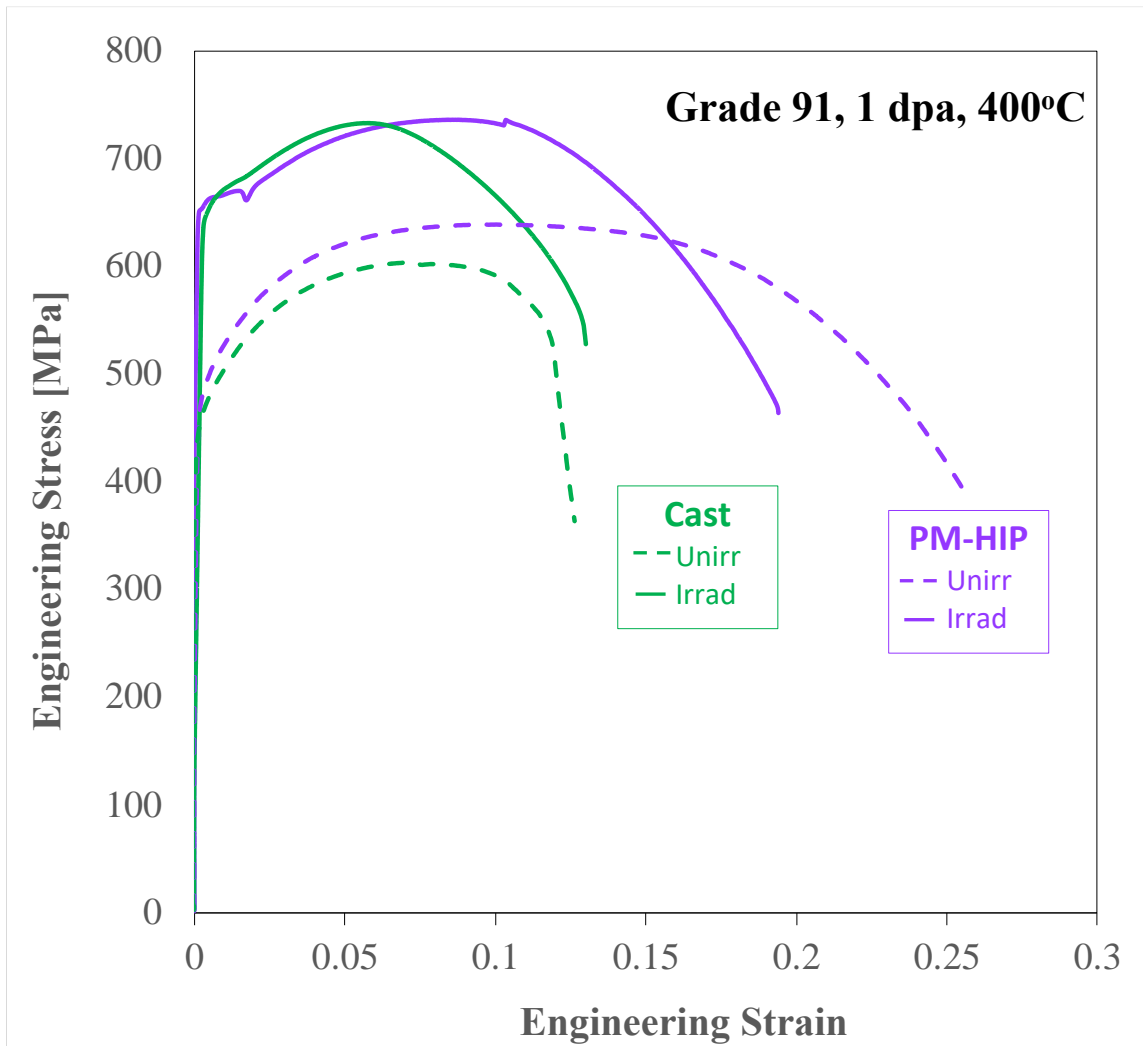


Figure 4.1. Stress- strain curves, where the cast is the green lines and PM-HIP is purple

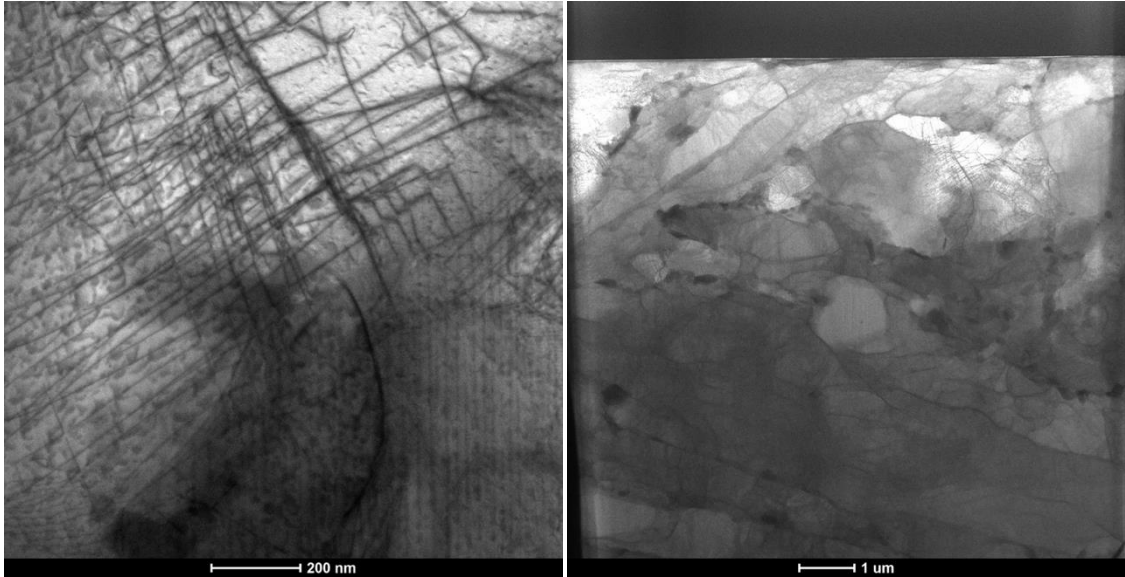


Figure 4.2. BFSTEM images of unirradiated Cast sample.



Figure 4.3. BFSTEM images of PM-HIP unirradiated sample.

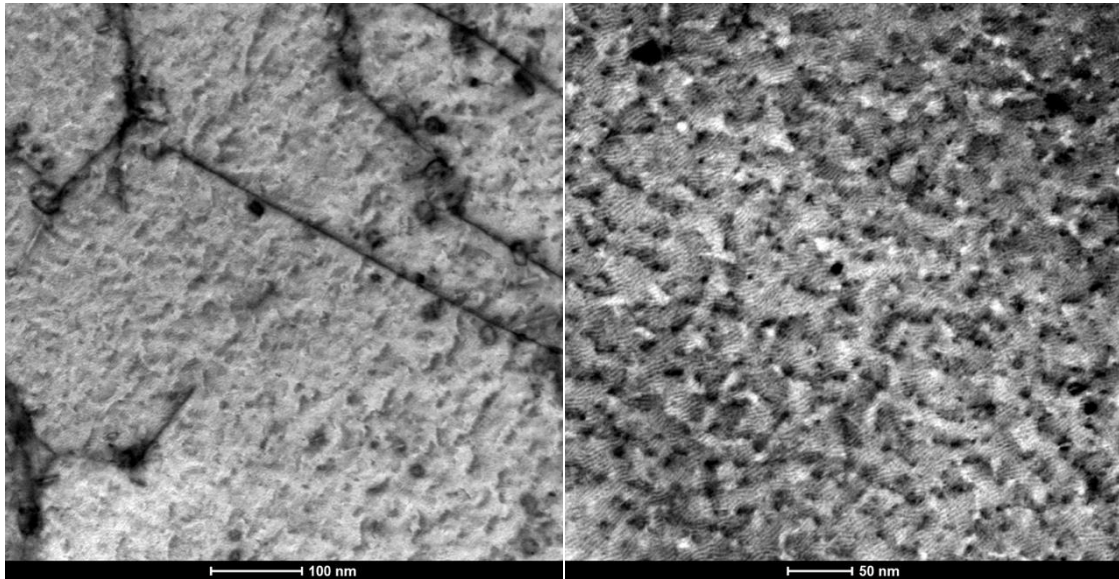


Figure 4.4. BFSTEM images of irradiated Cast sample.

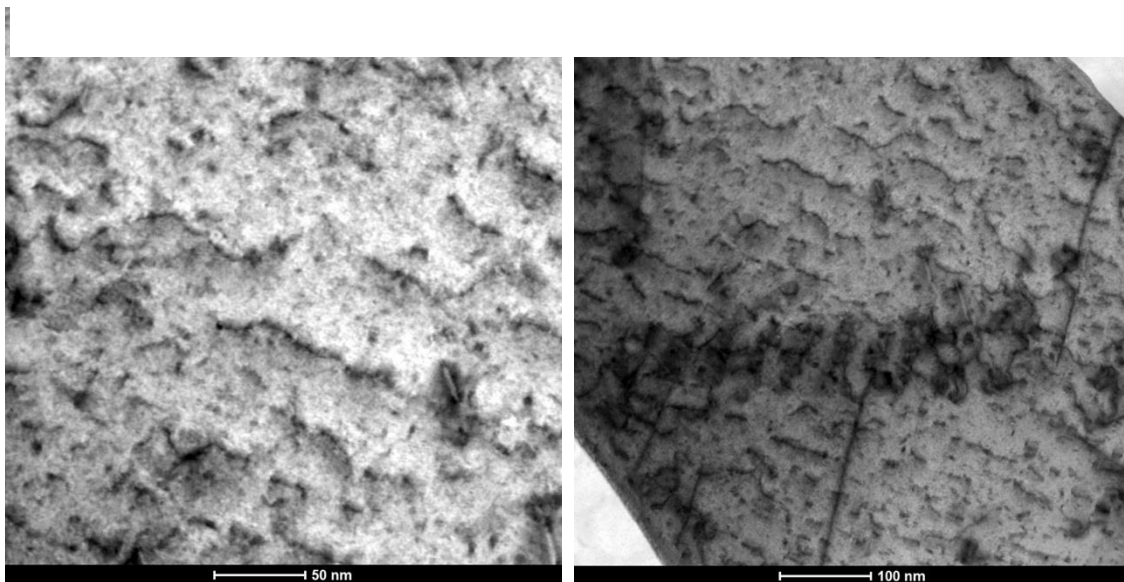


Figure 4.5. BFSTEM images of irradiated PM-HIP sample.

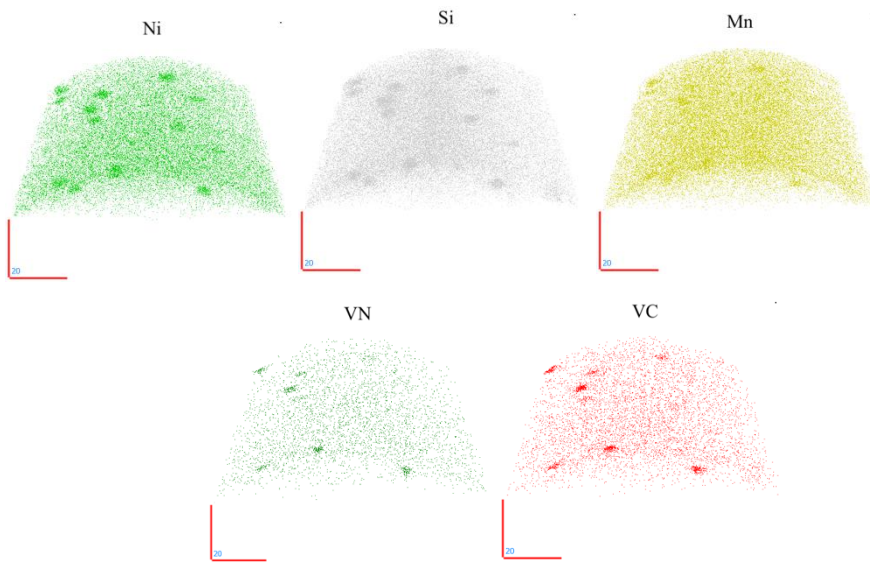


Figure 4.6. APT reconstructions of Cast R33\_10784 tip.

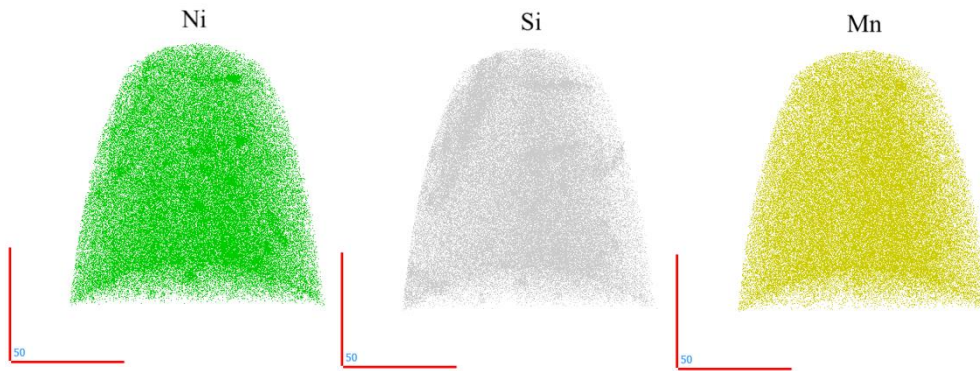


Figure 4.7. APT reconstructions of PM-HIP R33\_21502, shows slight Ni precipitation and Si segregation.

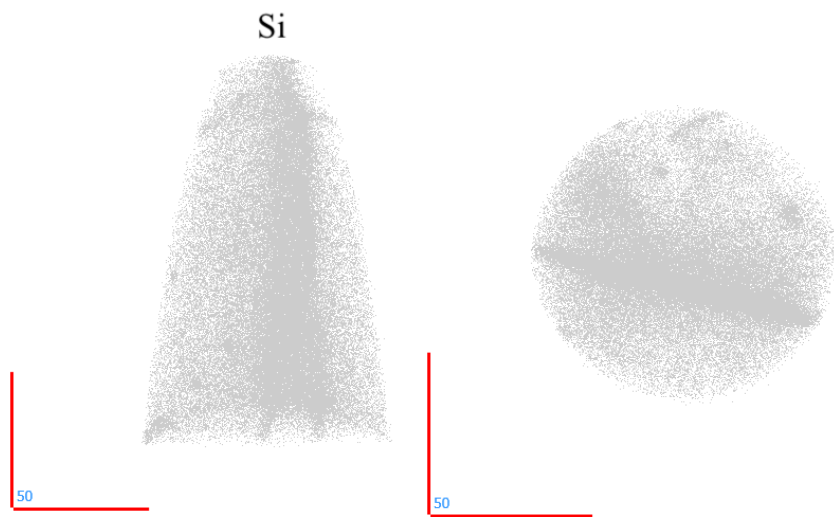


Figure 4.8. APT reconstructions of PM-HIP tip that shows significant Si segregation.

## 5. DISCUSSION

### 5.1 Increase in Yield Stress

As known irradiation causes an increase in yield stress through the formation of defects that strengthen the material. This was seen in both the PM-HIP and Cast samples. The increase in yield stress was calculated by subtracting the yield stress of unirradiated sample from the yield stress of the irradiated sample. For the PM-HIP sample the increase in yield stress was found as 271.75 MPa. For the Cast sample the increase in yield stress was found as 184.95 MPa. The higher yield stress of the PM-HIP alloy after irradiation further increases the interest in this alloy for nuclear applications.

### 5.2 Strengthening Calculations

Several different strengthening models were applied to calculate the contributions from the defects that were found in the material. As discussed in the introduction, most of the strengthening models are based off of the Dispersed Barrier Hardening Model. The strength factor makes a considerable difference in the value that the DBH model yields. This strength factor is based off of a variety of different aspects with regards to the shape and size. Tan and Busby proposed strength factors for loops and precipitates of various shapes. In another study involving a Fe-9%Cr ODS steel Swenson et al. proposed various methods for estimating the strength factor for loops and precipitates in this alloy that was neutron irradiated to 3 dpa at 500°C[45]. They found loops with a diameter around 8.9 nm and a number density of  $2.7 \times 10^{21} /\text{m}^3$ .

The oxide nanoclusters that were found through APT had an average diameter of 3.41 nm and a number density of  $43.5 \times 10^{22}/\text{m}^3$  [45]. When comparing these to the size and number density values found in the G91 samples, for loops and precipitates, it is seen that the G91 sample has significantly higher loop number density and loops with larger diameters. It can be reasonably suggested that the strength factor proposed in the study of the ODS alloy, of 0.44, for dislocation loops may not be the best estimate for the G91[45]. The calculated strength factor of 0.1, for the oxide nanoclusters however could be reasonable for the precipitates in G91 sample, as they have similar sizes and number densities.

Field et. al looked at a Fe-Cr-Al alloys, that were neutron irradiated at a dose of 1.8 dpa at 320°C[46]. 10Cr alloy in this study had similar composition to the G91 sample that was used in this thesis. Field also found dislocation loops with sizes around  $31.9 \text{ nm} \pm 18.7$ . These are somewhat comparable to the size of the dislocation loops found in the G91 samples. In order to calculate the strength factor for various defects they used a linear and sum-root square superposition formula. These formulas were dependent on the volume fraction, effective diameter, dislocation density of the defect[46]. Here they found  $\alpha$  as 0.17 for the  $a/2 \langle 111 \rangle$  dislocation loops. As Field's study was comparable to the G91 in this work, it was justifiable to use 0.17 as the strength factor when calculating the strengthening due to dislocation loops.

The strength factors of 0.1 and 0.17 were then applied in various strengthening models for precipitates and dislocation loops respectively. Equations 2.1, 2.2 2.3, 2.4 were all utilized to calculate the contribution to strengthening. The strengthening contributions from the various defects based on different models are summarized in [Error! Reference source not found.](#). It can be seen in the table that the potential contribution that could come from the SH model is not reasonable for the increase in yield stress from irradiation. So, while there does seem to be some level of unlocking in the tensile curves, this may not be the main strengthening mechanism involved.

The DBH for loops and precipitates for the Cast alloy seem to add up fairly closely to the  $\Delta\sigma_y$  found between irradiated and unirradiated Cast samples. The  $\Delta\sigma_y$  was 184.95 MPa as mentioned before, and the contribution from DBH of loops and precipitates is around 178.93 MPa. It is possible that there is some contribution from BKS or FKH models. Error could also be attributed to the dislocation loops and precipitates not being homogeneously distributed through the entire microstructure, though it was fairly homogenous in the areas where FIB lift outs were taken for STEM and APT. Any inaccuracies during the STEM loop measurement or APT reconstructions may also cause errors in strengthening calculations.

For the PM-HIP sample the contribution from DBH of loops and precipitates is around 106.22 MPa. This is lower than the overall  $\Delta\sigma_y$  found between irradiated and unirradiated PM-HIP samples. Part of this could be due to the heterogeneity of the microstructure that was observed from the areas the FIB lift outs were taken. Another reason could be strengthening due to Si, which will be discussed in the following section.

### 5.3 Si Segregation

As mentioned in the previous section there is a portion of the yield strength increase in the PM-HIP alloy that is not accounted for through the strengthening from dislocation loops and the precipitates found in that alloy. In Chapter 4 it was discussed that there was Si segregation seen in the almost all of the APT reconstructions of the PM-HIP alloy. Currently, it is unknown what feature the Si is segregating to, but regardless this segregation would still act as an obstacle for dislocation movement and therefore aid in increasing the yield strength of this alloy.

In a study done by Wharry et al. irradiation was done with 2MeV protons on a Fe-9Cr alloy, with similar chemistry to the G91, T91. Here they found that RIS occurred at prior austenite grain boundaries, but above 3 dpa redistribution occurs[47]. In this alloy it was also seen that dislocations were enriched in Si due to RIS. While this is not directly comparable to the work done in this thesis, as it was proton irradiation, it is notable that Si segregation does seem to be common in these alloys. This behavior was seen by Dubuisson et al as well, in several different ferritic martensitic steels[48]. They saw Ni and Si segregation ( $M_6C$ ) precipitates when there was more than 0.3% of these elements. However, they observed these precipitates to be more homogeneously distributed. In the G91 in this work, the heterogeneity of the Si segregation could be due to the PM-HIP processing. In another study by Xia et al. saw more Cr segregation in their F/M alloy, however from APT reconstructions, shown in the appendix, one can see that this was not present in the G91[25]. It is important to better characterize this segregation as it can lead to embrittlement, early failure, and possibly intergranular stress corrosion cracking[2]. Potential modeling on this could help create a better understanding of RIS in these alloys, which has not been thoroughly explored[23], [24].

Table 5.1. Summary of strengthening calculations.

	$\Delta\sigma_y$ (MPa)	DBH from precip. (MPa)	DBH from loops (MPa)	FKH loops (MPa)	SH from loops (MPa)	BKS loops (MPa) <sup>3</sup>
PM-HIP	271.75	79.54	26.68	1.22	576.868	1.37
Cast	184.95	69.572	109.36	9.56	785.298	4.74

## 6. CONCLUSION & FUTURE WORK

Gaining a better understanding of irradiation effects on PM-HIP alloys could be very useful in nuclear applications. The examination of two processing methods of G91 steel after neutron irradiation at 400°C to 1 dpa leads to the following conclusions:

1. Before irradiation the microstructures of the Cast and PM-HIP alloys contain mostly dislocation lines and very few loops. They seem to have fairly comparable microstructures prior to irradiation.
2. Post irradiation the Cast alloy contains clear decoration of dislocation loops along long dislocation lines. Irradiated PM-HIP alloy contains more loops than previously, but not as clear decoration of the loops along lines. The lines in the PM HIP were also much shorter. The PM-HIP microstructure is not as homogenous post irradiation as the Cast seems to be. The heterogeneity of the PM-HIP microstructure may be causing inaccuracies with measurements.
3. The increase in yield strength due to irradiation is higher in the PM-HIP alloy than the Cast alloy, which could be beneficial.
4. While the bulk of the strengthening comes from dislocation loops and precipitates, RIS could also be playing a role in the PM-HIP alloy.

The PM-HIP alloy does have a higher increase in yield stress due to irradiation. However, more work would need to be done to better characterize the microstructure as it is so heterogeneous in order to truly understand if it is suitable to be used for more widespread nuclear applications. There is a lot of work to be done in the PM-HIP space. The next steps in this research will be to understand the temperature and dose dependence of the irradiated microstructure. Both PM-HIP and Cast samples will be irradiated at 3 dpa and another set at 500°C to compare to the 1 dpa at 400°C. The same characterization through STEM, APT, and tensile testing will also be conducted on these new samples.

Another aspect that would be interesting to look at, on the current set and future samples would be fracture surfaces of irradiated and unirradiated samples from the tensile tests. STEM could be done on lamella from the fracture surfaces to better understand what defects and elements are present in those areas. This could potentially answer the question of whether or not the areas that Si has segregated to are the regions of fracture.

## APPENDIX: SUPPLEMENTARY FIGURES

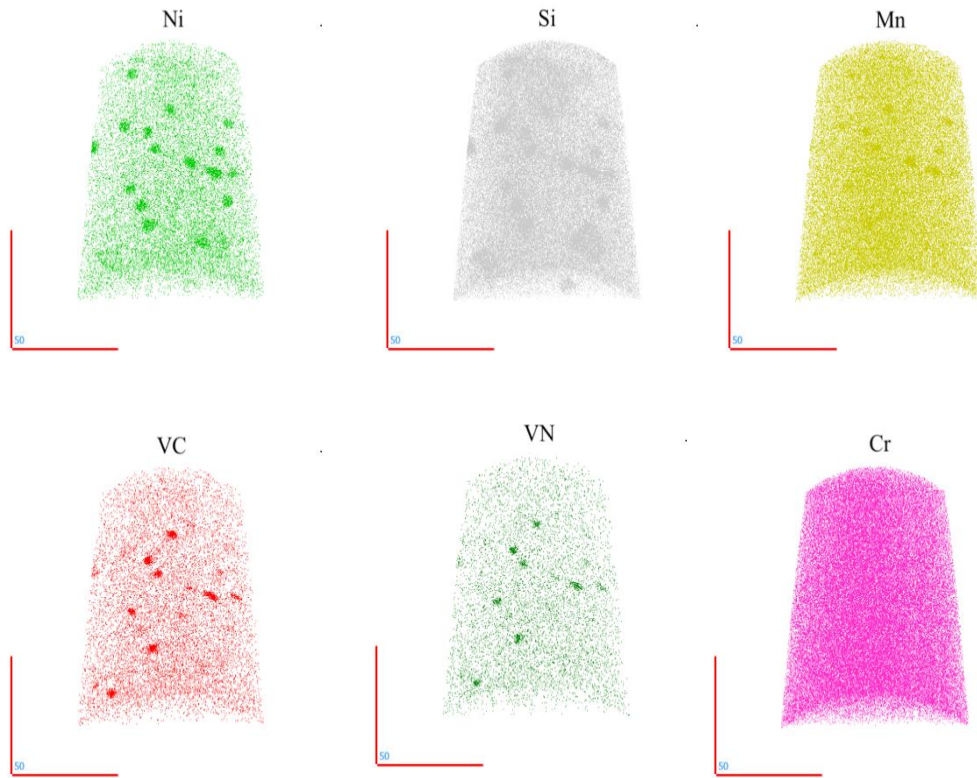


Figure A 1. Cast Tip R33\_10793 reconstruction. No Cr segregation is present.

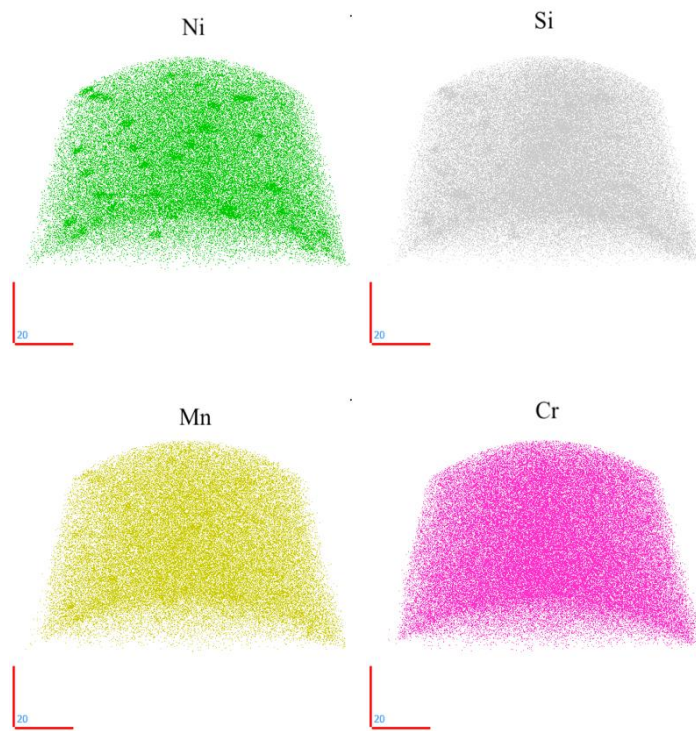


Figure A 2. PM-HIP Tip R33\_10777 reconstruction, shows slight Ni and Si precipitation, but no Cr precipitates.

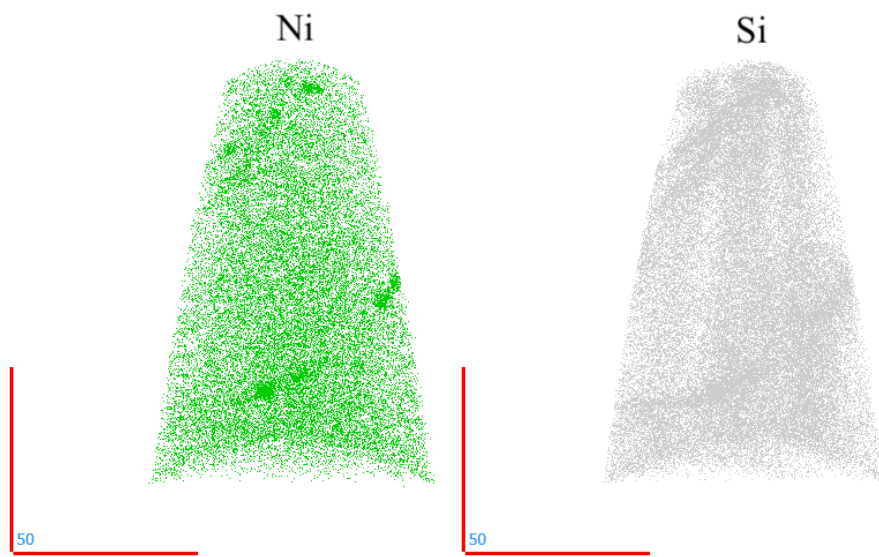


Figure A 3. PM-HIP Tip R33\_21474 reconstruction, showed only slight Ni precipitation and Si segregation.

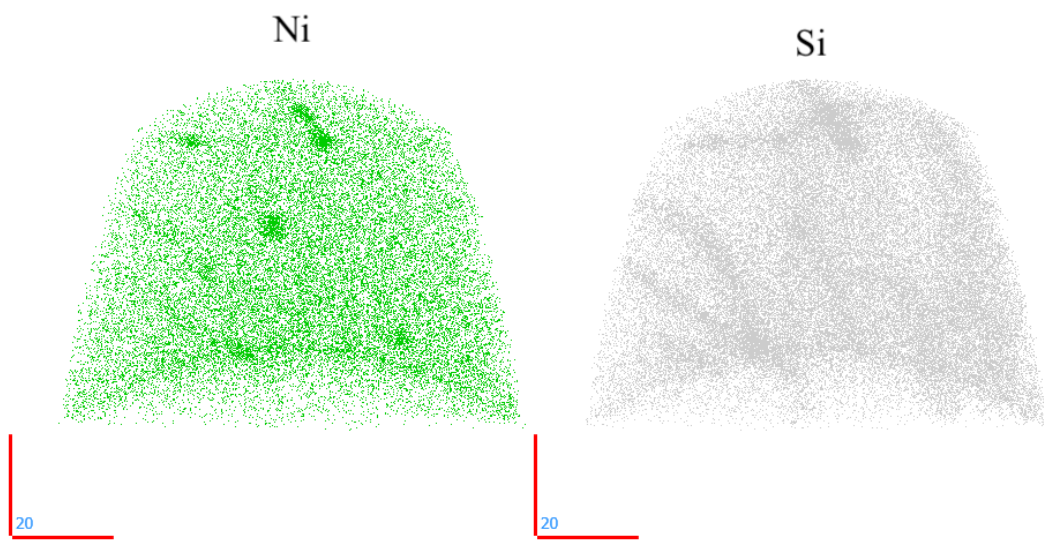


Figure A 4. PM-HIP Tip R33\_21475 reconstruction, showed only slight Ni precipitation and Si segregation.

## REFERENCES

- [1] H. Tas, S. Malang, F. Reiter, and J. Sannier, “Liquid breeder materials,” *Journal of Nuclear Materials*, vol. 155–157, pp. 178–187, Jul. 1988, doi: 10.1016/0022-3115(88)90239-5.
- [2] C. Cabet, F. Dalle, E. Gaganidze, J. Henry, and H. Tanigawa, “Ferritic-martensitic steels for fission and fusion applications,” *Journal of Nuclear Materials*, vol. 523, pp. 510–537, Sep. 2019, doi: 10.1016/j.jnucmat.2019.05.058.
- [3] R. L. Klueh and D. R. Harries, *High Chromium Ferritic and Martensitic Steels for Nuclear Applications*. 2001.
- [4] M. Samaras, “Nuclear Energy Systems: Advanced Alloys and Cladding,” in *Encyclopedia of Materials: Science and Technology*, Elsevier, 2011, pp. 1–7. doi: 10.1016/B978-0-08-043152-9.02263-6.
- [5] R. L. Klueh, K. Ehrlich, and F. Abe, “Ferritic/martensitic steels: promises and problems,” *Journal of Nuclear Materials*, vol. 191–194, pp. 116–124, Sep. 1992, doi: 10.1016/S0022-3115(09)80018-4.
- [6] V. Thomas Paul, S. Saroja, and M. Vijayalakshmi, “Microstructural stability of modified 9Cr–1Mo steel during long term exposures at elevated temperatures,” *Journal of Nuclear Materials*, vol. 378, no. 3, pp. 273–281, Sep. 2008, doi: 10.1016/j.jnucmat.2008.06.033.
- [7] J. A. Francis, W. Mazur, and H. K. D. H. Bhadeshia, “Review Type IV cracking in ferritic power plant steels,” *Materials Science and Technology*, vol. 22, no. 12, pp. 1387–1395, Dec. 2006, doi: 10.1179/174328406X148778.
- [8] C. Brown, V. Levy, J. L. Seran, R. J. Ehrlich, and J. C. Roger, “Fast Reactors and Related Fuel Cycles-FR’91,” 1991.
- [9] F. Abe, “Grade 91 heat-resistant martensitic steel,” in *Coal Power Plant Materials and Life Assessment*, Elsevier, 2014, pp. 3–51. doi: 10.1533/9780857097323.1.3.
- [10] Y. Z. Shen, S. H. Kim, H. D. Cho, C. H. Han, and W. S. Ryu, “Precipitate phases of a ferritic/martensitic 9% Cr steel for nuclear power reactors,” *Nuclear Engineering and Design*, vol. 239, no. 4, pp. 648–654, Apr. 2009, doi: 10.1016/j.nucengdes.2008.12.018.
- [11] F. Abe, M. Taneike, and K. Sawada, “Alloy design of creep resistant 9Cr steel using a dispersion of nano-sized carbonitrides,” *International Journal of Pressure Vessels and Piping*, vol. 84, no. 1–2, pp. 3–12, Jan. 2007, doi: 10.1016/j.ijpvp.2006.09.003.

- [12] R. L. Klueh and A. T. Nelson, “Ferritic/martensitic steels for next-generation reactors,” *Journal of Nuclear Materials*, vol. 371, no. 1–3, pp. 37–52, Sep. 2007, doi: 10.1016/j.jnucmat.2007.05.005.
- [13] F. Abe, M. Taneika, and K. Sawada, “Alloy design of creep resistant 9Cr steel using a dispersion of nano-sized carbonitrides,” *Int. J. Pressure Vessels Piping*, vol. 84, pp. 3–12, 2007.
- [14] X. Jia and Y. Dai, “Microstructure in martensitic steels T91 and F82H after irradiation in SINQ Target-3,” *Journal of Nuclear Materials*, vol. 318, pp. 207–214, May 2003, doi: 10.1016/S0022-3115(03)00101-6.
- [15] L. K. Mansur and G. R. Freeman, “Kinetics of nonhomogeneous processes,” in *Mechanisms and Kinetics of Radiation Effects in Metals and Alloys*, John Wiley & Sons, 1987.
- [16] M. J. Swenson and J. P. Wharry, “Nanocluster irradiation evolution in Fe-9%Cr ODS and ferritic-martensitic alloys,” *Journal of Nuclear Materials*, vol. 496, pp. 24–40, Dec. 2017, doi: 10.1016/j.jnucmat.2017.08.045.
- [17] Z. Jiao, V. Shankar, and G. S. Was, “Phase stability in proton and heavy ion irradiated ferritic–martensitic alloys,” *Journal of Nuclear Materials*, vol. 419, no. 1–3, pp. 52–62, Dec. 2011, doi: 10.1016/j.jnucmat.2011.08.020.
- [18] O. Anderoglu *et al.*, “Phase stability of an HT-9 duct irradiated in FFTF,” *Journal of Nuclear Materials*, vol. 430, no. 1–3, pp. 194–204, Nov. 2012, doi: 10.1016/j.jnucmat.2012.06.038.
- [19] American Nuclear Society., *Nuclear science and engineering : the journal of the American Nuclear Society*. Academic Press, 1956. Accessed: Mar. 18, 2022. [Online]. Available: [https://inis.iaea.org/search/search.aspx?orig\\_q=RN:52032401](https://inis.iaea.org/search/search.aspx?orig_q=RN:52032401)
- [20] C. Zheng, M. A. Auger, M. P. Moody, and D. Kaoumi, “Radiation induced segregation and precipitation behavior in self-ion irradiated Ferritic/Martensitic HT9 steel,” *Journal of Nuclear Materials*, vol. 491, pp. 162–176, Aug. 2017, doi: 10.1016/j.jnucmat.2017.04.040.
- [21] G. S. Was, *Fundamentals of radiation materials science: Metals and alloys, second edition*. Springer New York, 2016. doi: 10.1007/978-1-4939-3438-6.
- [22] T. R. Allen, J. T. Busby, G. S. Was, and E. A. Kenik, “On the mechanism of radiation-induced segregation in austenitic Fe–Cr–Ni alloys,” *Journal of Nuclear Materials*, vol. 255, no. 1, pp. 44–58, May 1998, doi: 10.1016/S0022-3115(98)00010-5.

- [23] H. Wiedersich, P. R. Okamoto, and N. Q. Lam, “A theory of radiation-induced segregation in concentrated alloys,” *Journal of Nuclear Materials*, vol. 83, no. 1, pp. 98–108, Aug. 1979, doi: 10.1016/0022-3115(79)90596-8.
- [24] G. S. Was *et al.*, “Assessment of radiation-induced segregation mechanisms in austenitic and ferritic–martensitic alloys,” *Journal of Nuclear Materials*, vol. 411, no. 1–3, pp. 41–50, Apr. 2011, doi: 10.1016/j.jnucmat.2011.01.031.
- [25] L. D. Xia *et al.*, “Radiation induced grain boundary segregation in ferritic/martensitic steels,” *Nuclear Engineering and Technology*, vol. 52, no. 1, pp. 148–154, Jan. 2020, doi: 10.1016/j.net.2019.07.009.
- [26] N. L. Loh and K. Y. Sia, “An overview of hot isostatic pressing,” *Journal of Materials Processing Technology*, vol. 30, no. 1, pp. 45–65, Feb. 1992, doi: 10.1016/0924-0136(92)90038-T.
- [27] D. W. Gandy *et al.*, “Small modular reactor vessel manufacture/fabrication using PM-HIP and electron beam welding technologies,” 2019. doi: 10.21741/9781644900031.
- [28] J. Anderson and R. Figliola, “Observations of Gas Atomization Process Dynamics , Modern Developments in Powder Metallurgy,” *Metal Powder Industries Federation* , pp. 205–223, 1988.
- [29] E. V. van Osch *et al.*, “Low temperature irradiation experiments and material testing in Petten,” *Journal of Nuclear Materials*, vol. 233–237, pp. 1541–1546, Oct. 1996, doi: 10.1016/S0022-3115(96)00134-1.
- [30] M. Carter *et al.*, “On the influence of microstructure on the neutron irradiation response of HIPed SA508 steel for nuclear applications,” *Journal of Nuclear Materials*, vol. 559, p. 153435, Feb. 2022, doi: 10.1016/j.jnucmat.2021.153435.
- [31] M. Jong *et al.*, “Post-irradiation characterization of PH13-8Mo martensitic stainless steel,” *Journal of Nuclear Materials*, vol. 417, no. 1–3, pp. 145–148, Oct. 2011, doi: 10.1016/j.jnucmat.2010.12.202.
- [32] T. H. Courtney, *Mechanical Behavior of Materials* , 2nd ed. Long Grove, Illinois: Waveland Press, 2000.
- [33] S. Queyreau, G. Monnet, and B. Devincre, “Orowan strengthening and forest hardening superposition examined by dislocation dynamics simulations,” *Acta Materialia*, vol. 58, no. 17, pp. 5586–5595, Oct. 2010, doi: 10.1016/j.actamat.2010.06.028.

- [34] G. E. Lucas, “The evolution of mechanical property change in irradiated austenitic stainless steels,” *Journal of Nuclear Materials*, vol. 206, no. 2–3, pp. 287–305, Nov. 1993, doi: 10.1016/0022-3115(93)90129-M.
- [35] L. Tan and J. T. Busby, “Formulating the strength factor  $\alpha$  for improved predictability of radiation hardening,” *Journal of Nuclear Materials*, vol. 465, pp. 724–730, Oct. 2015, doi: 10.1016/j.jnucmat.2015.07.009.
- [36] F. Bergner, M. Hernández-Mayoral, C. Heintze, M. J. Konstantinović, L. Malerba, and C. Pareige, “Tem observation of loops decorating dislocations and resulting source hardening of neutron-irradiated fe-cr alloys,” *Metals (Basel)*, vol. 10, no. 1, Jan. 2020, doi: 10.3390/met10010147.
- [37] D. J. Bacon, U. F. Kocks, and R. O. Scattergood, “The effect of dislocation self-interaction on the orowan stress,” *Philosophical Magazine*, vol. 28, no. 6, pp. 1241–1263, Dec. 1973, doi: 10.1080/14786437308227997.
- [38] F. Bergner, C. Pareige, M. Hernández-Mayoral, L. Malerba, and C. Heintze, “Application of a three-feature dispersed-barrier hardening model to neutron-irradiated Fe–Cr model alloys,” *Journal of Nuclear Materials*, vol. 448, no. 1–3, pp. 96–102, May 2014, doi: 10.1016/j.jnucmat.2014.01.024.
- [39] F. Kroupa and P. B. Hirsch, “Elastic interaction between prismatic dislocation loops and straight dislocations,” *Discuss Faraday Soc*, vol. 38, p. 49, 1964, doi: 10.1039/df9643800049.
- [40] X. Xiao, D. Terentyev, H. Chu, and H. Duan, “Theoretical models for irradiation hardening and embrittlement in nuclear structural materials: a review and perspective,” *Acta Mechanica Sinica*, vol. 36, no. 2, pp. 397–411, Apr. 2020, doi: 10.1007/s10409-020-00931-w.
- [41] ASTM International, “ASTM Standard E8, ‘Tension Testing of Metallic Materials.’” ASTM International, 2013.
- [42] L. A. Giannuzzi and F. A. Stevie, “A review of focused ion beam milling techniques for TEM specimen preparation,” *Micron*, vol. 30, pp. 197–204, 1999.
- [43] M. J. Swenson and J. P. Wharry, “The comparison of microstructure and nanocluster evolution in proton and neutron irradiated Fe–9%Cr ODS steel to 3 dpa at 500 °C,” *Journal of Nuclear Materials*, vol. 467, pp. 97–112, Dec. 2015, doi: 10.1016/j.jnucmat.2015.09.022.

- [44] B. H. Sencer, J. R. Kennedy, J. I. Cole, S. A. Maloy, and F. A. Garner, “Microstructural analysis of an HT9 fuel assembly duct irradiated in FFTF to 155dpa at 443°C,” *Journal of Nuclear Materials*, vol. 393, no. 2, pp. 235–241, Sep. 2009, doi: 10.1016/j.jnucmat.2009.06.010.
- [45] M. J. Swenson, C. K. Dolph, and J. P. Wharry, “The effects of oxide evolution on mechanical properties in proton- and neutron-irradiated Fe-9%Cr ODS steel,” *Journal of Nuclear Materials*, vol. 479, pp. 426–435, Oct. 2016, doi: 10.1016/j.jnucmat.2016.07.022.
- [46] K. G. Field, X. Hu, K. C. Littrell, Y. Yamamoto, and L. L. Snead, “Radiation tolerance of neutron-irradiated model Fe–Cr–Al alloys,” *Journal of Nuclear Materials*, vol. 465, pp. 746–755, Oct. 2015, doi: 10.1016/j.jnucmat.2015.06.023.
- [47] J. P. Wharry, Z. Jiao, V. Shankar, J. T. Busby, and G. S. Was, “Radiation-induced segregation and phase stability in ferritic–martensitic alloy T 91,” *Journal of Nuclear Materials*, vol. 417, no. 1–3, pp. 140–144, Oct. 2011, doi: 10.1016/j.jnucmat.2010.12.052.
- [48] P. Dubuisson, D. Gilbon, and J. L. Séran, “Microstructural evolution of ferritic-martensitic steels irradiated in the fast breeder reactor Phénix,” *Journal of Nuclear Materials*, vol. 205, pp. 178–189, Oct. 1993, doi: 10.1016/0022-3115(93)90080-I.